

## Strain gauge analysis of laser forming

S. P. Edwardson,<sup>a)</sup> K. G. Watkins, G. Dearden, and P. French  
*Department of Engineering, Laser Group, The University of Liverpool, Liverpool L69 3GH,  
United Kingdom*

J. Magee  
*National Centre for Laser Applications, NUI Galway, Ireland*

(Received 6 November 2002; accepted for publication 10 March 2003)

Laser forming has become a viable process for the shaping of metallic components, as a means of rapid prototyping and of adjusting and aligning. The laser forming process is of significant value to industries that previously relied on expensive stamping dies and presses for prototype evaluations. This investigation aims to complement the considerable amount of work already completed on two-dimensional laser forming, offering an insight into the mechanical behavior of a part during the process using a strain gauge analysis technique. The investigation was performed on mild steel CR4 sheet using a CO<sub>2</sub> laser source. It includes empirical investigations to determine optimum processing parameters using the temperature gradient mechanism, thermocouple analysis to locate ideal strain gauge placement for temperature compensation, and strain gauge analysis of the transverse localized strains at a number of locations on the surface of the sheet during single and multipass laser forming. The results of the investigation demonstrate the relative complexity of the process even during a simple straight-line bend and that a residual strain component remains in the sheet after processing. © 2003 Laser Institute of America.

Key words: laser forming, strain gauge analysis, thermocouple analysis, mild steel

### I. INTRODUCTION

This investigation is primarily concerned with the process of laser forming or laser bending of metal sheet material with a high power laser beam. Laser forming has become a viable process for the shaping of metallic components, as a means of rapid prototyping and of adjusting and aligning. The laser forming process is of significant value to industries that previously relied on expensive stamping dies and presses for prototype evaluations. Relevant industry sectors include aerospace, automotive, and microelectronics. In contrast with conventional forming techniques this method requires no mechanical contact and hence offers many of the advantages of process flexibility associated with other laser manufacturing techniques such as laser cutting and marking.<sup>1</sup> Laser forming can produce metallic, predetermined shapes with minimal distortion. The process is similar to the well established torch flame bending used on large sheet material in the ship building industry but a great deal more control of the final product can be achieved.<sup>2</sup> The laser forming process is realized by introducing thermal stresses without melting into the surface of a work piece. These internal stresses induce plastic strains, bending or shortening the material, or result in a local elastic plastic buckling of the work piece depending on the mechanism active.<sup>3</sup>

The range of metals that can be laser formed is considerable. As there is only localized heating involved below the melting temperature, the bulk properties are not altered and good metallurgical properties are retained in the irradiated

area.<sup>4,5</sup> Materials of particular interest are specialized high strength alloys.<sup>6</sup> These include titanium and aluminum alloys. These materials are widely used in the aerospace industry where the implementation of laser bending as a replacement of existing manufacturing processes is under investigation,<sup>7,8</sup> as well as other industry areas.<sup>9</sup>

### II. EXPERIMENT

This investigation aims to complement the considerable amount of work already completed on two-dimensional laser forming, offering an insight into the mechanical behavior of a part during the process using a strain gauge analysis technique. The investigation was performed on 80×80 mm and 80×200 mm 1.5 mm gauge mild steel CR4 (AISI 1010) coupons using a high power CO<sub>2</sub> laser source. It includes empirical investigations on the 80×80 mm coupons to determine optimum processing parameters using the temperature gradient mechanism (TGM).<sup>3</sup> Also included is thermocouple analysis to locate ideal strain gauge placement and strain gauge analysis of the transverse localized strains at a number of locations on the surface of the 80×200 mm coupons during multipass laser forming. The longer coupons used provide sufficient area to attach the strain gauges.

#### A. Background—the TGM<sup>3</sup>

This mechanism is the most widely reported, and can be used to bend sheet material out of plane towards the laser. The conditions for the temperature gradient mechanism are energy parameters that lead to a steep temperature gradient across the sheet thickness. This results in a differential ther-

<sup>a)</sup>Electronic mail: s.p.edwardson@liverpool.ac.uk

mal expansion through the thickness. The beam diameter is typically of the same order as the sheet thickness. The path feed rate has to be chosen to be large enough that a steep temperature gradient can be maintained. The feed rate and hence the temperature gradient has to be increased if materials are used which have a high thermal conductivity. The laser path on the sheet surface is typically a straight line across the whole sheet. This straight line coincides with the bending edge. Initially the sheet bends in the direction away from the laser. This is called counter bending. With continued heating the bending moment of the sheet opposes the counter bending and the mechanical properties of the material are reduced. Once the thermal stress reaches the temperature dependent yield stress any further thermal expansion is converted into plastic compression. During cooling the material contracts again in the upper layers, and because it has been compressed, there is a local shortening of the upper layers of the sheet and the sheet bends towards the laser beam. The yield stress and Young's modulus return to a much higher level during this cooling phase and little plastic re-straining occurs. Bends of approximately  $1^\circ$  per pass are achieved with this mechanism.<sup>1</sup>

## B. Experimental setup

An ElectroX™ 1.5 kW CO<sub>2</sub> laser, wavelength 10.6  $\mu\text{m}$ , run in continuous wave mode was used for the forming process. The laser beam was fed via turning mirrors to a set of X-Y-Z CNC tables for beam manipulation. The mild steel coupons were laser cut to the correct dimensions in order reduce any prestressing that might influence the forming results. To prepare them for forming they were first cleaned with acetone in order to remove an oil film that protected them from oxidation. They were then sprayed with graphite in order to increase the absorption of the 10.6  $\mu\text{m}$  radiation. The coupons were clamped 30 mm from the scan line along one edge during processing using an aluminum clamp as can be seen in Fig. 1. A laser range finder was used to record height data either side of the irradiation line and hence determine the bend angle after each pass, the sensor can be seen to the right of the processing head in Fig. 1. Combined with software based control of the CNC axes and shutter the system is fully automated, producing bend angle output to file after each pass.

The thermocouple analysis of a multipass strategy was performed using K type thermocouples, which have a range of  $-200$ – $1370^\circ\text{C}$ . The thermocouples were attached to the top and bottom surface of the  $200 \times 80$  mm coupons along a center line at a number of locations 10–58 mm away from the laser irradiation line on the free end using adhesive pads. An Agilent 34970A data acquisition unit was used to record the temperature data from the thermocouples, acquiring data at up to 250 readings/s. The temperature data were then used to determine strain gauge placement, based on operating temperature and adverse thermal gradient.

The strain gauge analysis was performed using polyimide backed 5 mm long uniaxial foil gauges, which have a temperature range of  $-30$ – $180^\circ\text{C}$ , in this range the gauge factor  $K$  is constant. The gauges selected were temperature

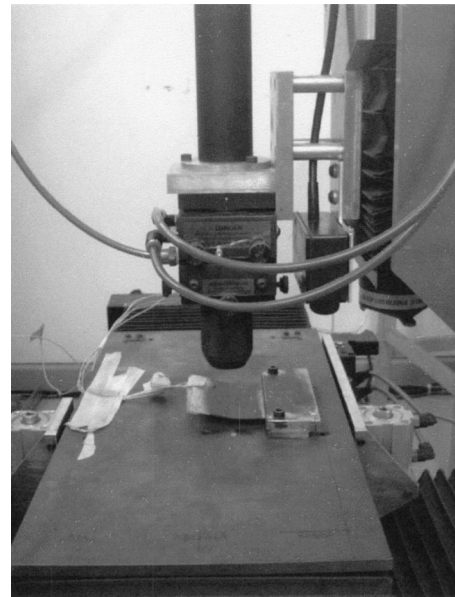


FIG. 1. Experimental setup.

compensated for the thermal expansion of mild steel. The gauges were each incorporated into a balanced and zeroed quarter Wheatstone bridge circuit (Fig. 2) the output of which was amplified by a four channel bridge amplifier and recorded, thus allowing four single strain gauges to be monitored at any one time.

Although the gauges could be arranged to give the net bending strains or temperature compensation in half or full bridge configurations, it was thought that due to the asymmetry of the laser forming process the determination of the average localized strains would yield more meaningful results. The gauges were located in a perpendicular orientation to the laser scan line to measure the transverse thermally induced strains at locations at or near the longitudinal center line and 10 mm from the edges of the coupon. The distances from the laser scan line were decided upon by the results of the thermocouple analysis, locations on the top and bottom surfaces of the coupons where the peak temperatures are within the operating range of the gauges. The gauges were attached to the keyed and cleaned surface of the coupons using a Cyanoacrylate adhesive and can be seen in Fig. 3.

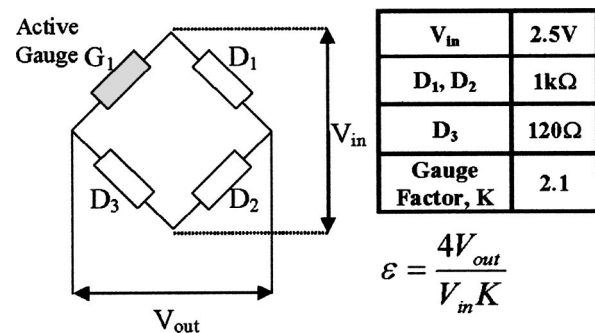


FIG. 2. Quarter bridge circuit.

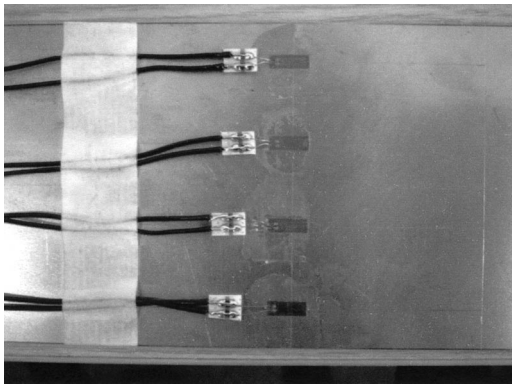


FIG. 3. Strain gauges attached to a coupon.

### III. RESULTS AND DISCUSSION

#### A. Determination of ideal processing parameters

This investigation used the 80×80 mm 1.5 mm gauge mild steel CR4 coupons to identify ideal processing parameters using the temperature gradient mechanism to be used for strain gauge analysis, employing a multipass alternating direction strategy at 60 s intervals and recording the bend angle per pass. Three beam diameters were investigated; 3, 5.5, and 8 mm inducing various energy fluences to establish a process window and identify a maximum achievable bend angle per pass and after 30 passes. The bend angles with increasing numbers of scans at various energy fluences are shown in Figs. 4, 5, and 6.

As can be seen in Figs. 4–6 it is possible to identify for each chosen beam diameter a speed/power combination for maximized forming. The graphs indicate an increase in bend angle per pass with an increase in energy fluence. Figure 7 shows a comparison of the maximized bend angle for each beam diameter at a constant power of 760 W. As can be seen after 30 passes, the parameters achieving the highest bend angle are a beam diameter of 8 mm and a traverse speed of 20 mm/s. However as the TGM is unlikely to be the active mechanism at this energy fluence, the process parameters chosen for the strain gauge analysis were the next lowest fluence: laser power 760 W, beam diameter 5.5 mm, and a traverse speed of 30 mm/s. It can also be observed in Figs. 4–7 that a decreasing rate of bending occurs with increasing numbers of scans. This has been attributed to a number of

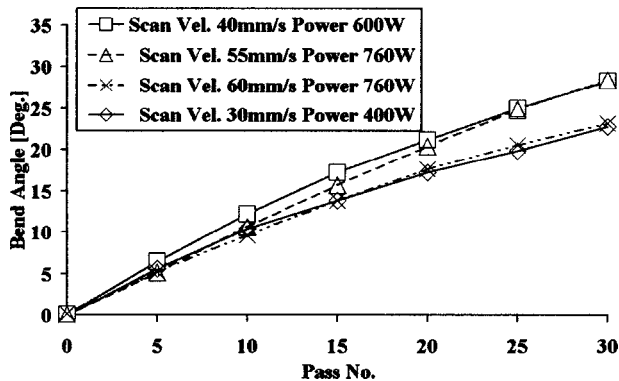


FIG. 4. 3 mm beam diam results.

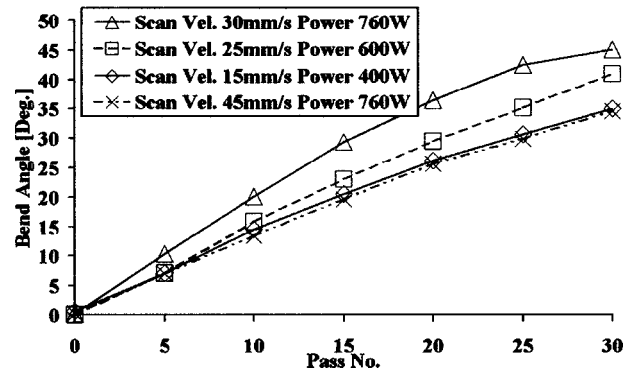


FIG. 5. 5.5 mm beam diam results.

factors including strain hardening,<sup>10</sup> section thickening,<sup>11</sup> coating burnoff, and an increase in bulk material temperature reducing the thermal gradient achievable.

#### B. Thermocouple analysis

A thermocouple investigation was performed using the chosen processing parameters to ensure ideal strain gauge placement. The thermocouples were attached to the top and bottom surfaces of an 80×200 mm coupon at 10, 22, 34, 46, and 58 mm away from the laser irradiation line (Fig. 8). The temperature data from six laser passes of alternating direction at 60 s intervals was recorded. The results are shown in Fig. 9.

As can be seen in Fig. 9 the peak temperature after six passes at the closest location, 10 mm is 115 °C. This is well within the operating range of the strain gauges. It can also be noted that there is very little difference in temperature between the top and bottom surfaces at identical distances from the scan line, thus it would follow that strain gauges at those locations should see similar thermal strains. It was therefore decided to center the strain gauges at 10 and 46 mm away from the scan line, regions of high and low thermal gradients across the surfaces. It can also be noted from Fig. 8 that the peak temperatures near the scan line steadily increase per pass as the bulk material temperature increases. It can be assumed that a similar effect occurs along the scan line itself making it possible to melt the surface if left unchecked. This suggests a need for additional cooling of the component. An

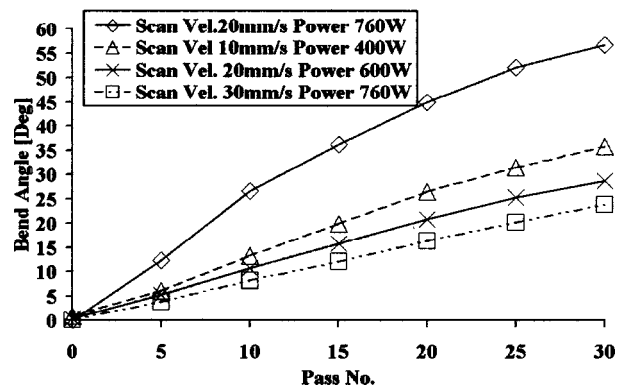


FIG. 6. 8 mm beam diam results.

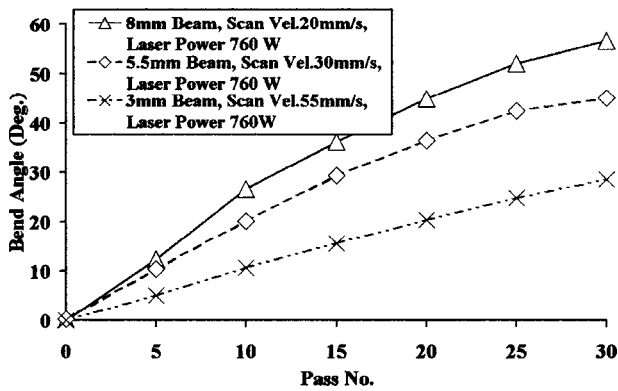


FIG. 7. Maximized forming comparison at 760 W.

increase in the bulk material temperature also leads initially to an improved bending rate per pass, in that a heated coupon is easier to plastically deform. However as the bulk temperature increases the attainable thermal gradient across the thickness of the sheet decreases for the same energy parameters.

**C. Strain gauge analysis**

As discussed, the strain gauges were located on the top and bottom surfaces at 10 and 46 mm away from the center of the laser scan line, at or near the longitudinal center line and 10 mm from either edge of the coupons (Fig. 10). As the output from only four gauges could be logged at any one time, a separate coupon was used for each configuration. An assumption was made that the process conditions were identical for each sample as each coupon was laser cut from the same mild steel sheet. The output from the gauges at 46 mm on the top surface is shown in Figs. 11, 12, 13, and 14 and the output from the bottom surface is shown in Figs. 15, 16, 17, and 18. The gauge locations are given as distances from the first edge of the 80 mm wide plates on the first pass of six using an alternating direction strategy.

Figures 12, 13, 16, and 17 show the output from the strain gauges around the center of the plate. Figures 11, 14, 15, and 18 show the output from the two edges on the top and bottom surfaces at 46 mm from the scan line. A positive strain value indicates a tensile component and a negative value a compressive component. It can be seen that even at

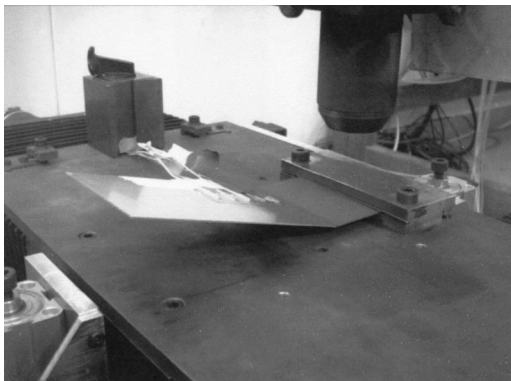


FIG. 8. Thermocouple analysis setup.

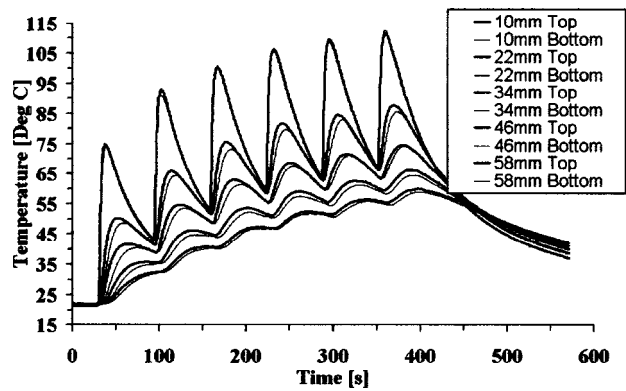


FIG. 9. Thermocouple data, 6 pass, 760 W, 5.5 mm Ø, 30 mm/s.

this relatively large distance from the irradiation line a small but significant strain measurement can be made, the peak range being in the region of 18 microstrain. It can also be seen that there is a considerable difference in the strain output at the center of the plate compared to the edges. At the center of the plate on the top surface (Figs. 12 and 13) a tensile component (perhaps due to thermal expansion) is seen during each pass that recovers initially to a residual tensile strain. Then, as the number of passes increases an increasing residual compressive strain is seen, which recovers somewhat several minutes after processing. At the plate edges on the top surface (Figs. 11 and 14) an initial tensile component changes to a compressive component during each pass and a tensile residual strain develops sometime after processing. On the bottom surface similar strain outputs to the top surface from the center (Figs. 16 and 17) to the edges (Figs. 15 and 18) of the plate are seen. However at the center the magnitudes of the induced tensile strains are less than the top surface but there is still a residual compressive strain component after processing. At the plate edges on the bottom surface the initial tensile component during processing is less than that at the top surface and the recovery after processing is to an increasing residual compressive strain. The residual strains on the bottom surface appear to recover several minutes after processing upon cooling. It can also be noted in all of the results at a distance of 46 mm that the effect of the

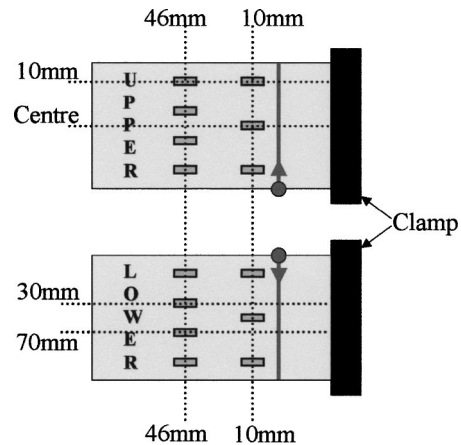


FIG. 10. Schematic showing strain gauge locations.

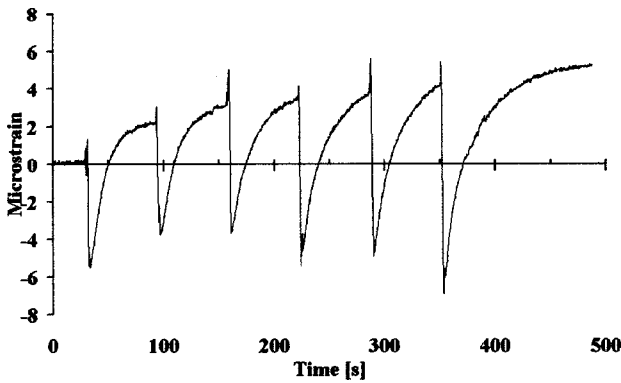


FIG. 11. Strain gauge output at 46 mm top surface, 10 mm from first edge.

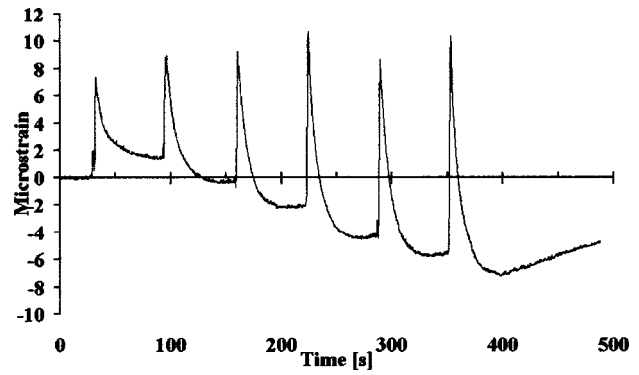


FIG. 13. Strain gauge output at 46 mm top surface, 50 mm from first edge.

alternating processing direction is a variation in the peak values depending on the direction.

To summarize the results at 46 mm from the scan line for the 200×80 mm plates, it can be seen that compressive strains are generated near the center of the plate and tensile strains at the edges on the top and bottom surfaces during processing. The residual strain components appear to recover upon cooling, however a residual tensile component is observed at the edges on the top surface.

These results appear consistent with the observed edge effect<sup>12</sup> or longitudinal bowing phenomenon where it is thought that a change in boundary conditions from the center to the edge of the plate results in a variation in bend angle from edge to edge. If a different in-process strain cycle occurs and hence a different residual transverse strain state exists between the center and the edge of the plate and top and bottom surfaces, then this could possibly explain this edge effect distortion. Further investigation is necessary to determine the longitudinal strains during laser forming, as this should aid the explanation of the edge effect distortion still further.

The output from the gauges at 10 mm from the irradiation line on the top surface is shown in Figs. 19, 20, and 21 and the output from the bottom surface is shown in Figs. 22, 23, and 24. As there was a very similar output from the centrally located strain gauges at 46 mm, it was decided to use a single strain gauge on the center line and two further gauges 10 mm from each edge at 10 mm from the scan line.

As with the output at 46 mm, Figs. 19–24 show a difference in strain output from the center to the edge and between top and bottom surfaces at 10 mm from the scan line, however there was a significant difference in output between the two locations. An initial observation was the expected increase in strain values recorded closer to the scan line. The range is now in the region of 100 microstrain. Figure 19 shows the transverse strain data 10 mm from the first edge on the top surface in the alternating direction irradiation strategy. It can be seen that on the first pass and subsequent odd numbered passes that there is a large tensile component consistent with thermal expansion as the beam passes that point followed by a recovery sometime after processing. On the return second pass and subsequent even numbered passes, however, there is an initial compressive strain that switches to a tensile strain as the beam reaches the other side of the plate followed again by a recovery to an increasing residual tensile strain component. On the opposing side of the plate (Fig. 21) the reverse occurs. On the first pass and subsequent odd numbered passes the output from the gauge furthest way from the laser beam starting position shows initially a compressive strain that switches to a tensile strain as the beam reaches that point, followed by recovery to a tensile residual strain component. On the second and subsequent even numbered passes a large tensile component is seen as the beam passes followed by a recovery. It can be seen (Figs. 19 and 21) that the residual tensile strain component present in both edges after six passes appears to be decreasing some time after processing. As the plate is cooling the purely elastic

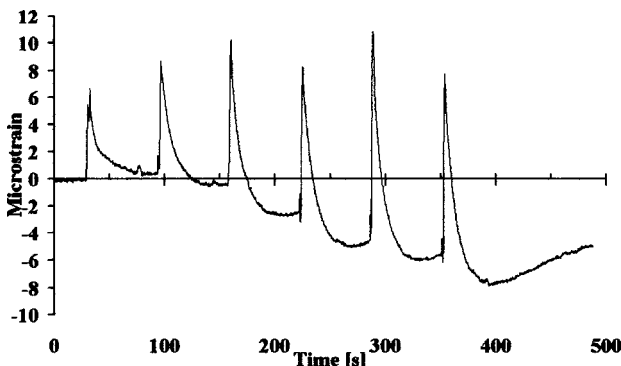


FIG. 12. Strain gauge output at 46 mm top surface, 30 mm from first edge.

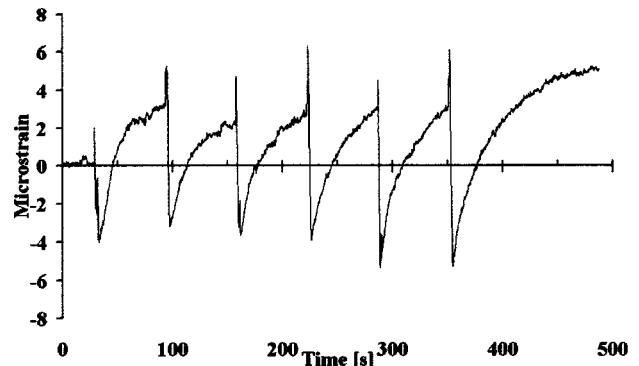


FIG. 14. Strain gauge output at 46 mm top surface, 70 mm from first edge.

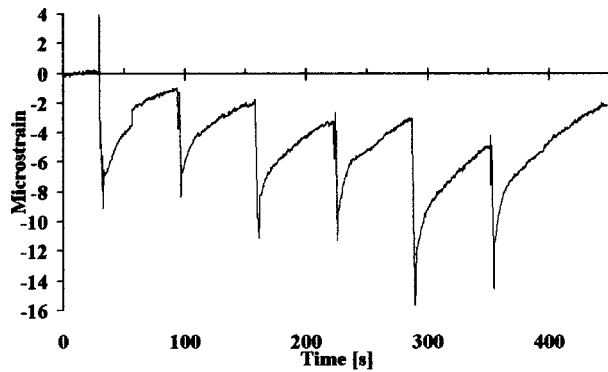


FIG. 15. Strain gauge output at 46 mm bottom surface, 10 mm from first edge.

strains are relieved. At the center of the plate, Fig. 20, it can be seen that there is a compressive or less tensile strain component during each pass which recovers to an increasing residual tensile strain that appears constant sometime after processing. The effect of the alternating direction strategy appears not to occur at the center line. The residual tensile strain observed in the top surface close to the scan line may be due to the plastic compression and hence transverse shortening in the irradiated area consistent with the TGM.

Figures 22, 23, and 24 show the output from the gauges positioned on the bottom surface 10 mm from the irradiation line. In Figs. 22 and 24 it can be seen that as with the top surface the edges on the bottom are affected by the asymmetry of the process and the traverse direction. At the edge closest to the start point of the laser (Fig. 22) on the first pass and subsequent odd numbered passes a compressive strain is seen initially, consistent with the upper surface expansion and counter bend. This rapidly reverts to a tensile component as the beam moves to the other side of the plate. On the reverse second pass and subsequent even numbered passes a tensile strain component is seen that reverts rapidly to a compressive or less tensile strain then recovers to a higher residual tensile strain. The tensile component remaining in the sheet after processing appears constant sometime after processing. On the opposing side of the sheet (Fig. 24) the sequence is mirrored; the edge furthest away from the laser start position sees a tensile strain initially that rapidly changes to a less tensile state as the laser reaches that loca-

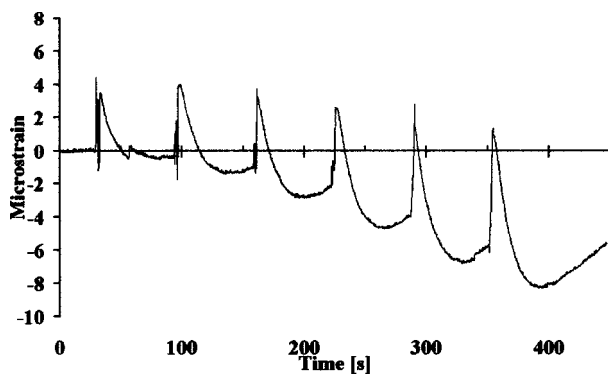


FIG. 16. Strain gauge output at 46 mm bottom surface, 30 mm from first edge.

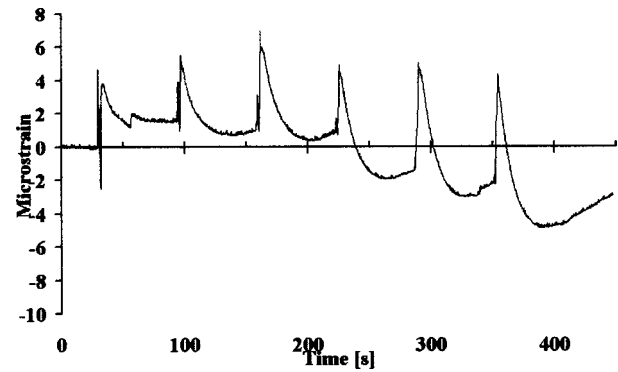


FIG. 17. Strain gauge output at 46 mm bottom surface, 50 mm from first edge.

tion followed by a recovery to a residual higher tensile strain. The edge closest to the laser start position sees a compressive strain initially that rapidly reverts to a tensile strain as the beam traverses to the other side of the plate. There is a residual tensile strain on this edge as well. It can be noted though from Figs. 22 and 24 that the magnitude of this strain depends on the direction of the final pass. At the center location on the bottom surface (Fig. 23), the gauge records evenly the effects at both edges, in that a tensile strain is seen as the beam moves across the plate and this reverts to a compressive strain as the beam passes the center and moves to the other side of the plate. This effect has been noted in other studies.<sup>13</sup> Again a recovery to a residual tensile strain occurs after processing due perhaps to the development of the bend toward the laser, which is consistent with the TGM theory.<sup>3</sup>

The strain gauge results demonstrate the complexity of the laser forming process even during a simple straight line two-dimensional (2D) bend. A large factor in this is the inherent asymmetry of the process when using a single point laser source to achieve a symmetrical solution. While absolute readings of strain are difficult at such high thermal gradients the general trends in strains due to thermal and mechanical influences have been revealed. It has been shown that along an irradiation line depending on where the beam is and its direction, there is a mechanical effect in the plate ahead and to the rear. Figures 25 and 26 show a visualization

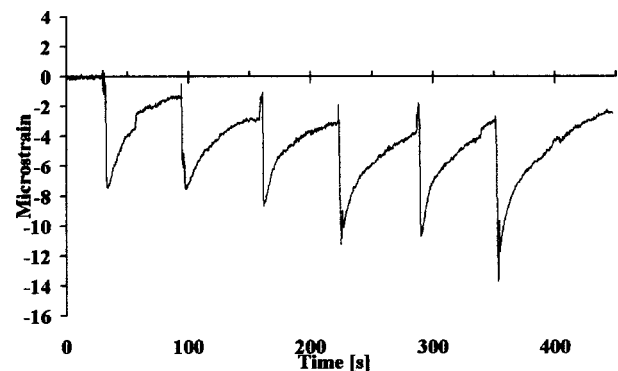


FIG. 18. Strain gauge output at 46 mm bottom surface, 70 mm from first edge.

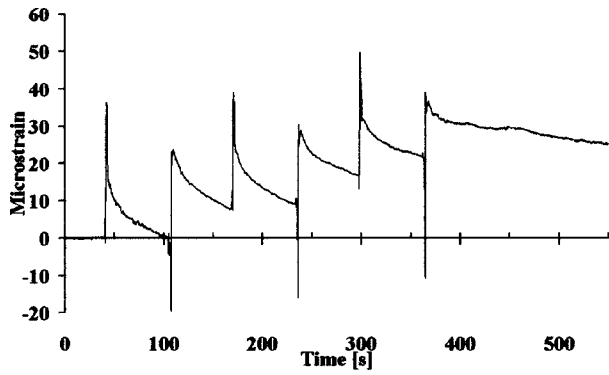


FIG. 19. Strain gauge output at 10 mm top surface, 10 mm from first edge.

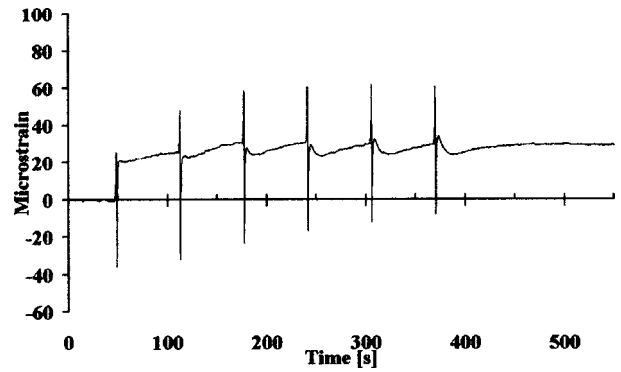


FIG. 23. Strain gauge output at 10 mm bottom surface, 40 mm from first edge (center line).

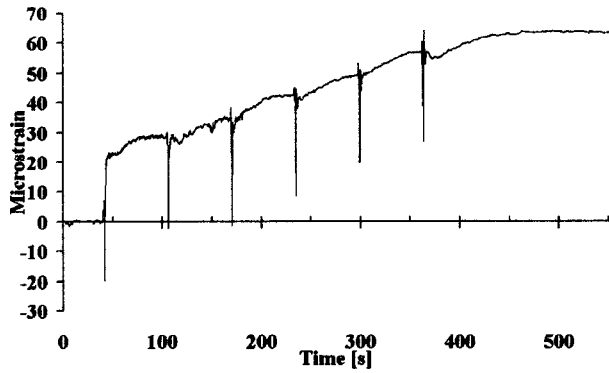


FIG. 20. Strain gauge output at 10 mm top surface, 40 mm from first edge (center line).

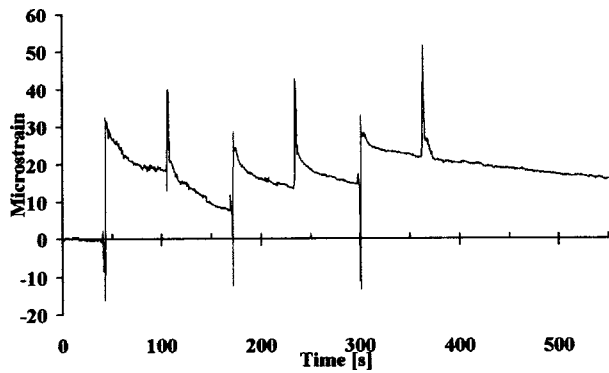


FIG. 21. Strain gauge output at 10 mm top surface, 70 mm from first edge.

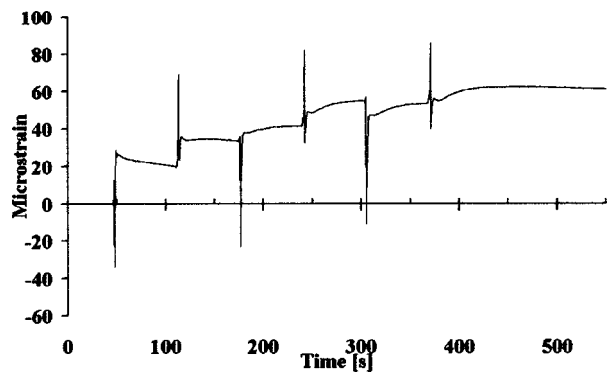


FIG. 22. Strain gauge output at 10 mm bottom surface, 10 mm from first edge.

of the results obtained from the strain gauges at either edge, top and bottom surfaces, 10 mm from the scan line at the start and end of a pass. The beam at the first edge causes a thermal expansion of the upper surface and hence a compression of the lower surface consistent with a counter bend effect. As one side of the plate expands a compression of the top surface of the other side of the plate is seen, perhaps due to a moment generated in the upper surface (Fig. 25). An opposing moment may be present in the lower surface, as one side is under compression a tensile strain is seen in the other side; this would suggest a torsion force is present in the plate between the top and bottom surfaces. As the beam reaches the other side of the plate (Fig. 26) the effect of a reversal in this moment may be evident by the sudden reduction in the tensile strain component of the first edge before a recovery of the elastic strains during cooling (Fig. 19).

A residual tensile strain was observed at 10 mm from the scan line on the bottom surface and along the center line on the top surface. The tensile component left in the bottom surface is consistent with the mechanical bend in the plate; the component in the top surface may be due to a transverse shortening of the upper surface along the scan line consistent with TGM theory.

#### IV. CONCLUSIONS

The results of the strain gauge analysis investigation demonstrate the complexity of the laser forming process

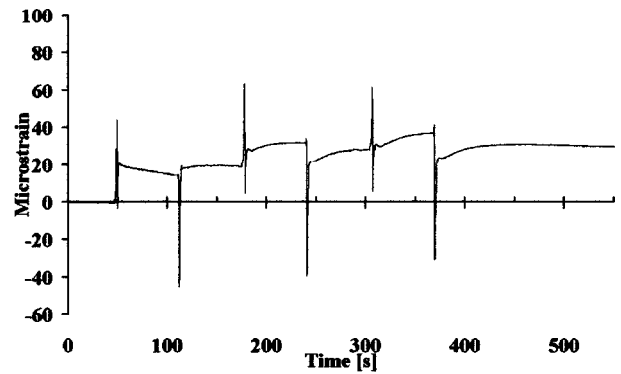


FIG. 24. Strain gauge output at 10 mm bottom surface, 70 mm from first edge.

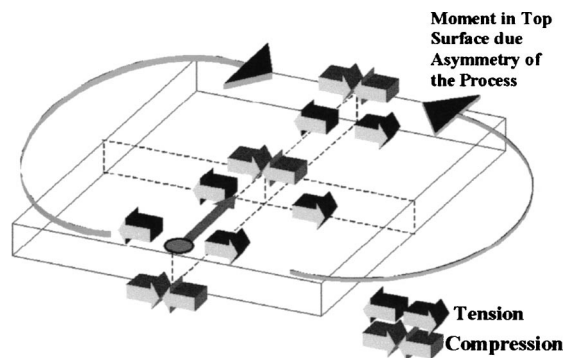


FIG. 25. Visualization of the strain output close to the scan line at the start of a pass.

even during a simple straight line 2D bend. A large factor in this is the inherent asymmetry of the process when using a single point laser source to achieve a symmetrical solution. It has been shown that along an irradiation line depending on where the beam is and its direction, there is a mechanical effect in the plate ahead and to the rear. While absolute readings of strain are difficult at such high thermal gradients the general trends in transverse localized strains due to thermal and mechanical influences have been revealed. A significant

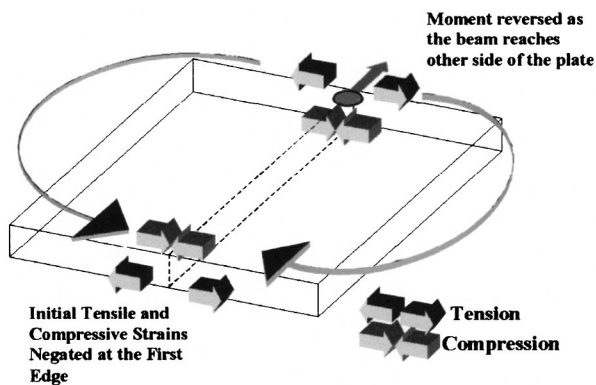


FIG. 26. Visualization of the strain output close to the scan line at the end of a pass.

difference in strain output was recorded at the plate edges when compared to the center on the top and bottom surfaces close to and distant from the scan line consistent with edge effect phenomenon.

## ACKNOWLEDGMENTS

The authors gratefully acknowledge the assistance given by BAE Systems, Rolls-Royce, and the EPSRC during this investigation.

- <sup>1</sup>J. Magee, K. G. Watkins, and W. M. Steen, "Advances in laser forming," *J. Laser Appl.* **10**, 235–246 (1998).
- <sup>2</sup>A. Moshaiov and W. Vorus, "The mechanics of the flame bending process, theory and applications," *J. Ship Res.* **31**, 269–281 (1987).
- <sup>3</sup>F. Vollertsen, "Forming, sintering and rapid prototyping," *Handbook of the Eurolaser Academy*, edited by D. Schuöcker (Chapman & Hall, London, 1998), pp. 357–453.
- <sup>4</sup>W. Maher, K. Tong, C. Bampton, M. Bright, J. Wooten, and C. Rhodes, "Laser forming of titanium and other metals is useable within metallurgical constraints," Proceedings of ICALEO'98, Orlando, FL, November 16–19, 1998. Section E, 1998, pp. 121–130.
- <sup>5</sup>J. Shackel, J. Sidhu, and P. B. Prangnell, "The metallurgical implications of laser forming Ti-6AL-4V sheet," Proceedings of ICALEO'2001, Jacksonville FL, October 2–5, 2001. Section D, 2001.
- <sup>6</sup>J. Magee, K. G. Watkins, and W. M. Steen, "Laser bending of high strength alloys," *J. Laser Appl.* **10**, 149–155 (1998).
- <sup>7</sup>J. Magee, K. G. Watkins, W. M. Steen, R. L. Cooke, and J. Sidhu, "Development of an integrated laser forming demonstrator system for the aerospace industry," Proceedings of ICALEO'98, Orlando, FL, November 16–19, 1998. Section E, 1998, pp. 141–150.
- <sup>8</sup>S. P. Edwardson, K. G. Watkins, G. Dearden, and J. Magee, "Generation of 3D shapes using a laser forming technique," Proceedings of ICALEO'2001, Jacksonville, FL, October 2–5, 2001, Section D, 2001.
- <sup>9</sup>R. J. Blake, R. M. Pearson, and A. B. Revell, "Laser thermal forming of sheet metal parts using desktop laser systems," Proceedings of ICALEO'97, Section E, 1997, pp. 66–75.
- <sup>10</sup>A. Sprenger, F. Vollertsen, W. M. Steen, and K. G. Watkins, "Influence of strain hardening on laser bending," *Manuf. Syst.* **24**, 215–221 (1995).
- <sup>11</sup>J. Magee, K. G. Watkins, W. M. Steen, N. Calder, J. Sidhu, and J. Kirby, "Edge effects in laser forming," Proceedings of the Laser Assisted Net Shape Engineering, Meisenbach Bamberg, Germany, 1997.
- <sup>12</sup>K. G. Watkins, S. P. Edwardson, J. Magee, G. Dearden, P. French, R. L. Cooke, J. Sidhu, and N. Calder, "Laser forming of aerospace alloys," *Proceedings of the SAE Aerospace Manufacturing Technology Conference, 2001* (Aerospace Congress, Seattle, 2001), Paper No. 2001-01-2610.
- <sup>13</sup>K. Scully, "Laser line heating," *J. Ship Prod.* **3**, 237–246 (1987).